

The Chandra ACIS Survey of M33 (ChASeM33): Transient X-ray Sources Discovered in M33

Benjamin F. Williams¹, Terrance J. Gaetz², Frank Haberl, Wolfgang Pietsch³, Avi Shporer⁴, Parviz Ghavamian⁵, Paul P. Plucinsky², T. Mazeh⁴, Manami Sasaki², and Thomas G. Pannuti⁶

ABSTRACT

The *Chandra* ACIS Survey of M33 (ChASeM33) has acquired 7 fields of ACIS data covering M33 with 200 ks of exposure in each field. A catalog from the first 10 months of data, along with archival *Chandra* observations dating back to the year 2000, is currently available. We have searched these data for transient sources that are measured to have a 0.35-8.0 keV unabsorbed luminosity of at least 4×10^{35} erg s⁻¹ in one epoch and are not detected in another epoch. This set of the survey data has yielded seven such sources, including one previously-known supersoft source. We analyzed *XMM-Newton* data from the archive distributed over the years 2000 to 2003 to search for recurrent outbursts and to get a spectrum for the supersoft transient. We find only one recurrent transient in our sample. The X-ray spectra, light curves, and optical counterpart candidates of two of the other sources suggest that they are high-mass X-ray binaries. Archival *Spitzer* photometry and high X-ray absorption suggest that one of the sources is a highly variable background active galactic nucleus. The other three sources are more difficult to classify. The bright transient population of M33 appears to

¹University of Washington Astronomy Department, Box 351580, Seattle, WA, 98195; ben@astro.washington.edu

²Harvard-Smithsonian Center for Astrophysics, 60 Garden Street, Cambridge, MA 02138; gaetz@ead.cfa.harvard.edu; plucinsk@head.cfa.harvard.edu; msasaki@cfa.harvard.edu

³Max-Planck-Institut für extraterrestrische Physik, 85741 Garching, Germany; fwh@mpe.mpg.de; wnp@mpe.mpg.de

⁴Wise Observatory, Raymond and Beverly Sackler Faculty of Exact Sciences, Tel Aviv University, Tel Aviv 69978, Israel; shporer@wise.tau.ac.il; mazeh@wise.tau.ac.il

⁵Department of Physics and Astronomy, Johns Hopkins University, 3400 North Charles Street, Baltimore, MD 21218; parviz@pha.jhu.edu

⁶Space Science Center, Morehead State University, 200A Chandler Place, Morehead, KY 40351; t.pannuti@morehead-st.edu

contain a large fraction of high-mass X-ray binaries compared with the transient populations of M31 and the Galaxy, reflecting the later morphology of M33.

Subject headings: X-rays: binaries — galaxies: individual (M33) — binaries: close — X-rays: stars

1. Introduction

X-ray transient sources are rare and valuable laboratories for the study of accretion physics. Most low-mass X-ray binaries that are observed as transient X-ray sources have been shown to contain black hole primaries (McClintock & Remillard 2006). These objects, known as black hole binaries (BHBs), are of great interest for studies of disk accretion in the strong gravity regime. Other transient events come from supersoft sources (SSSs; e.g. Di Stefano et al. 2004, and references therein), which are likely to harbor white dwarf primaries (King et al. 2002). Still other transient events occur in high-mass X-ray binaries (HMXBs); these have hard spectra and often have neutron star primaries. Most such systems are *Be* transients driven by wind-fed accretion (Tanaka & Shibazaki 1996).

While there has been a significant amount of research dedicated to observing and understanding the transient X-ray sources discovered in the Galaxy (McClintock & Remillard 2006; Jain et al. 2001; Tomsick et al. 2005, and many others), relatively little work has been done to compare this population of exotic sources to their extragalactic analogs. Most of the existing extragalactic studies concentrate on transients in the Magellanic Clouds (Coe et al. 2001; Kahabka & Pietsch 1996) and M31 (see Williams et al. 2006b, and references therein). Studies of M31 suggest that the black hole/neutron star (BH/NS) ratio in M31 could be higher than expected from simple stellar evolution and that the transient rate in M31 is comparable to or slightly higher than that of the Galaxy (Williams et al. 2004). The Magellanic Clouds do not contain large samples of LMXB transient sources, but the Small Magellanic Cloud contains a large number of *Be* binaries for its size (Haberl & Pietsch 2004).

Because of its excellent spatial resolution ($\sim 1''$ FWHM at 1 keV) and its ability to revisit the same part of the sky at several different times of the year, the *Chandra* X-ray Observatory is particularly well-suited to conduct searches for transient X-ray sources in nearby galaxies. Based on its low distance modulus of $(m - M)_0 = 24.50$ (van den Bergh 1991) and low inclination angle of 56 degrees (Zaritsky et al. 1989), the nearby spiral galaxy M33 is a prime target for such searches. Compared to more distant spiral galaxies or larger nearby spirals, M33 is relatively easy to fully monitor with *Chandra*, allowing classification of the transient sources as well as comparisons of the M33 transient population with those

of the Galaxy and M31.

Our *Chandra* Very Large Program (VLP) to survey M33 to a depth of $\sim 5 \times 10^{34}$ erg s $^{-1}$ with the ACIS-I array (Pietsch et al. 2006; Gaetz et al. 2007; Plucinsky et al. 2008; , ApJS, submitted) is providing a wealth of data covering nearly all of the M33 disk at a variety of epochs. While we were not able to control the depth and coverage of these epochs to optimize the data set for creating an unbiased sample of X-ray transients, our data are still extremely useful for discovering new transient sources. We therefore have carefully searched our first source catalog (Plucinsky et al. 2008) and the Grimm et al. (2005) *Chandra* catalog for the brightest transient sources in order to provide some detailed information about the characteristics of transient X-ray sources in M33.

In this paper, we announce the discovery that six of the new X-ray sources cataloged by the ChASeM33 survey are transient sources, and we discuss our analysis of a seventh, previously-known transient. Two of the candidates have optical counterpart candidates with the color and brightness of upper main sequence stars in M33, making them likely to be high-mass X-ray binaries (HMXBs). One candidate has a very red counterpart, suggesting that it is a low-mass X-ray binary. Two more have faint optical counterpart candidates, and the rest have no detected optical counterparts.

2. Data Analysis

2.1. *Chandra*

The data for this study were obtained from the *Chandra* Archive and the ChASeM33 project. The data included in this study as well as the initial data processing steps and source detection are discussed in detail in Plucinsky et al. (2008). We produced light curves for all of the sources in both the Grimm et al. (2005) and Plucinsky et al. (2008) catalogs using the software package *ACIS Extract* (Broos et al. 2002). This software package is optimized to perform measurements of sources observed with AXAF CCD Imaging Spectrometer (ACIS) multiple times with different off-axis angles, and different detector chips. The output provides photon fluxes and errors from each exposure as well as upper-limits for non-detections and a spectrum for each source that combines the multiple exposures, taking into account the different sensitivities and point spread functions of different locations on the array. Furthermore, the output provides short-term variability information by running a Kolmogorov-Smirnov (K-S) test against a constant photon arrival rate during the brightest detection.

The long-term light curves of all of the sources were calculated from the *ACIS Extract*

output starting with the number of counts within an aperture that enclosed 90% of the energy in the point spread function at the source’s location on the detector in each individual observation. The local background was calculated from a surrounding source-free area of the detector large enough to capture 50 counts. The background counts were then scaled to the appropriate area and subtracted from the total counts. The net counts were converted to photon flux using the exposure maps created by the ChASeM33 team (Plucinsky et al. 2008).

This photon flux from each observation was then converted to a luminosity estimate using a conversion factor of 2.7×10^{41} erg cm² photons⁻¹, which corresponds to the unabsorbed 0.35–8 keV luminosity of a source with photon index $\Gamma \sim 1.7$ and $N_H=10^{21}$ cm⁻². Such spectral parameters are typical for X-ray transient sources (Williams et al. 2006b). The value chosen did not affect our results, because our selection criteria were determined based on relative fluxes, not absolute luminosities. We adopt this luminosity conversion to make the criteria that we used more meaningful to the reader.

We selected transient sources based on two criteria: first, the maximum luminosity, which corresponds to the luminosity the source was required to have in at least one observation; second, the minimum luminosity ratio, which corresponds to the ratio h/l , where h is the maximum luminosity measured for a source in a single observation and l is the upper-limit on the faintest luminosity measured at the location of the source in a single observation. This ratio was required to be larger than the adopted value for a source to be considered as a transient candidate. A grayscale plot of the number of sources passing our selection criteria as a function of the values of those criteria is shown in Figure 1, where darker gray corresponds to more sources passing the transient criteria. The number of transient candidates rises steeply in the region centered at a maximum unabsorbed 0.35-8 keV luminosity cutoff of $\sim 4 \times 10^{35}$ erg s⁻¹ and a h/l cutoff of ~ 8 . We therefore adopted these values to create our initial candidate list.

Based on these results, we flagged point sources that were (1) detected in at least one observation with an unabsorbed 0.35-8 keV luminosity of $> 4 \times 10^{35}$ erg s⁻¹ (1.5×10^{-6} ph cm⁻² s⁻¹) at $\geq 4\sigma$ significance, (2) not detected at 1.5σ significance in another observation, and (3) had an upper-limit that was at least a factor of 8 fainter than the maximum luminosity. Errors were taken to be the standard deviation of the number of counts, making the definition of a non-detection more conservative than under the Gehrels approximation (Gehrels 1986), which yields larger errors and decreases the significance of detections. This selection yielded 8 initial candidates.

Each observation of these candidates was then scrutinized by eye to look for photometry problems as well as a visible detection and non-detection. One of the initial candidates had

contamination from a neighboring source and was therefore removed from the sample. This final culling produced 7 transient candidates. The positions of these sources are shown in Figure 2, and the light curves are shown in Figure 3. Images taken when these transient candidates were detected at 4σ significance are shown beside images taken when the transient candidates were not detected in Figure 4. Table 1 lists their observed properties.

Two of the seven candidates were previously cataloged by *Chandra* or *XMM-Newton*. These include XRT-2, which is source 145 in the catalog of Misanovic et al. (2006), and XRT-6, which is the previously-known supersoft transient source 207 in the catalog of Misanovic et al. (2006). This latter source is also identified as source J013409.9+303219 in the catalog of Grimm et al. (2007). The fact that our search recovered Misanovic et al. (2006) #207 independently suggests that our technique returns robust X-ray transient candidates.

We checked the literature for potential optical counterparts for our transient candidates. We compared the ChASem33 positions of X-ray sources with known optical counterparts (taken from Hatzidimitriou et al. 2006; Misanovic et al. 2006; Shporer & Mazeh 2006) to their coordinates in the Massey et al. (2006) catalog. The resulting average shift between ChASem33 and Massey et al. (2006) coordinates was $\Delta R.A. = -0.45 \pm 0.38''$ and $\Delta Dec. = -0.21 \pm 0.39''$, which is insignificant and consistent (within the errors) with the typical ChASem33 catalog positional error of $0.3''$. We therefore assume no systematic offset in our search for counterparts, but we did include an extra error component of $0.5''$ (added in quadrature to our X-ray position errors in Table 1) to account for errors in alignment between optical and X-ray positions. Since this component of the error is specific to the X-ray alignment with the Massey et al. (2006) data, it is only included in comparisons with this dataset, not in the *Chandra* position errors provided in Table 1.

2.2. *XMM-Newton*

We analyzed the relevant portions of the *XMM-Newton* survey of M33 obtained from 2000 to 2003 to search for recurrent outbursts of our transient candidates and to help constrain the spectral properties of XRT-6. The individual *XMM-Newton* observations were shorter by about a factor of 10 than the *Chandra* observations and therefore the *Chandra* data provided tighter constraints on the upper limits for the transient sources. All measurements were obtained using the archival *XMM-Newton* data processed as detailed in Misanovic et al. (2006). Upper-limits were taken as the flux necessary for a source with a spectrum of $\Gamma=1.7$ (assuming a column density of $N_H = 6 \times 10^{20} \text{ cm}^{-2}$) to provide a detection $\geq 3\sigma$ above the background.

In two cases, *XMM-Newton* data were not of sufficient spatial resolution to obtain reliable upper-limits for the transient candidate when the corresponding nearby source was active (XRT-3 and XRT-4). Our inspections of the *XMM-Newton* data showed no evidence for X-ray sources at the locations of XRT-1, XRT-5, or XRT-7, the best upper-limits for these candidates in any *XMM-Newton* observation were $\sim 3 \times 10^{35}$ erg s $^{-1}$ ($\sim 10^{-6}$ ph cm $^{-2}$ s $^{-1}$) for an energy range of 0.2-4.5 keV. In addition, even though XRT-2 was detected by *XMM-Newton* (Misanovic et al. 2006) with a flux of 2.8×10^{-15} erg cm $^{-2}$ s $^{-1}$, the source could be transient. The non-detection of this source comes from an archival *Chandra* observation (OBSID 1730), which was taken 2000-Jul-12. The detections of Misanovic et al. (2006) come from *XMM-Newton* observations of their field 15 on 2002-Jan-27 (see Misanovic et al. 2006, Table 1). Therefore, while we were able to determine that only XRT-2 and XRT-6 were active during any of the *XMM-Newton* observations of M33. XRT-2 was detected in outburst by *XMM-Newton* about 3 years before the ChASeM33 detection indicating a recurrent nature of the source.

We also made use of the *XMM-Newton* EPIC-pn data pertaining to the SSS XRT-6 in order to better constrain its spectral and temporal parameters. Spectra were extracted using single-pixel events which dominate at the low energies of interest. Although the number of net source counts is low (~ 220 counts between 0.2 and 0.6 keV on 2000-Aug-02 and ~ 105 counts on 2000-Aug-04) their confinement to a narrow energy band allows us to derive characteristic temperatures from a simple absorbed blackbody model fit. Light curves in the 0.2-0.6 keV band were extracted from the EPIC-pn data. The light curve binned to 200 s from 2000-Aug-02 (taken with thick optical blocking filter) with about 50% higher average count rate as compared to 2000-Aug-04 (medium filter) is shown in Figure 6.

2.3. Spitzer

We searched for mid-infrared counterparts to the seven X-ray transient candidates in archival Spitzer observations of M33. The entire galaxy was mapped with the IRAC instrument (Guaranteed Time Observation program 5; R. Gehrz, PI) between 2004 and 2006, with 6 observations targeting the inner 30' of M33. The IRAC instrument (Fazio et al. 2004) features four imagers centered at 3.6, 4.5, 5.8 and 8.0 μm (channels 1 through 4) with mean pixel scales of approximately 1''22. Each sequence in the M33 observations consisted of 483 frames per channel with a 3 point, 1/2-pixel dither for each position. The exposure time per pixel in each channel was 12 s. A preliminary analysis of data from this program is presented by Block et al. (2007).

We utilized the 16 August 2004 IRAC observation of M33 (Astronomical Observation

Request ID 3638784) to search for mid-infrared (mid-IR) counterparts. The data used were the downloaded image mosaics from the S14.0 version of the SSC pipeline. We performed a visual search for mid-IR counterparts to the seven X-ray transient candidates by overlaying the positions of the X-ray sources onto the four IRAC mosaics. We found mid-IR counterparts to four of the transient candidates (Table 2), though only one source (XRT-7) was detected in all four IRAC channels. We used SExtractor (Bertin & Arnouts 1996) version 2.3b2 to detect sources and perform photometry on the images. Stellar crowding in the outskirts of M33, where the seven X-ray transient candidates are located, is not severe in the IRAC images. We found that most of the default parameters for SExtractor were sufficient for detecting most of the point sources in the X-ray transient candidate fields. The parameters we adjusted were the minimum number of pixels needed for detection (DETECT_MINAREA = 3), the size of the region used to compute the background (BACK_SIZE = 32) and the background filtering size (BACK_FILTERSIZE = 3). In addition, we specified a local computation of backgrounds for each source (BACKPHOTO_TYPE = LOCAL).

The input photometric parameters for SExtractor included the instrumental gain for each channel, and the magnitude zero points as defined in the Vega system by Reach et al. (2005) and the IRAC version 3 data handbook. We used the isophotal magnitudes (MAGAUTO) output by SExtractor, computed from an aperture 5 pixels in radius and a background annulus 24 pixels thick. We then applied the aperture correction factor for each channel documented in the IRAC data handbook to obtain the final magnitude estimates.

3. Results

3.1. Spectra

The results of our ACIS Extract total flux measurements are supplied in Table 1 in the three ChASem33 bands (Plucinsky et al. 2008): 0.35-1.1 keV (soft), 1.1-2.6 keV (medium), and 2.6-8 keV (hard). These fluxes are the weighted mean fluxes of all observations of each source. The SSS XRT-6 had no flux in the hard or medium band and is poorly fit by an absorbed power-law model. The best-fit photon index $\Gamma=9.5$ reflects the supersoft nature of the source. XRT-3 had no flux in the hard band ($\leq 2.5 \times 10^{-7}$ photons $\text{cm}^{-2} \text{s}^{-1}$) and was poorly fit by a power-law model. XRT-2, XRT-5, and XRT-7 exhibited flux in all bands and have equivalent soft Γ values. XRT-1 and XRT-4 appear to be yet another spectral class, with most of their flux in the hard band. Similarly, their Γ values are hard, with values typical of those seen in HMXBs (e.g., Haberl & Pietsch 2004).

Fits to the spectra of the transient candidates were performed with XSPEC 12.0 (Fig-

ure 5), initially assuming a power-law with absorption. For the candidates with good power-law fits ($\chi^2/\nu < 1.5$; XRT-2, XRT-4, XRT-5, and XRT-7), we adopted the power-law as the correct spectral model. Otherwise, we attempted to find better-fitting models. If our data did not constrain the errors of a parameter to better than a factor of 2, we do not quote errors for that parameter.

Since the power-law fits to the spectra of XRT-1, XRT-3, and XRT-6, had large χ^2/ν values, we fit the spectra with some other models to gain additional insight into their nature. The spectrum extracted for XRT-1 was difficult to fit because of its hardness and strong emission at ~ 3 keV (see Figure 5). Because of this data point, fits to the spectrum with thermal models were no better than the original power-law fit. We therefore accepted the power-law model parameters when estimating the source peak luminosity given in Table 1.

The extracted spectrum of XRT-3 was best fit by either an absorbed disk blackbody or an absorbed blackbody model, suggesting that this transient candidate was in the high (thermal) state during the high flux observation. Since the disk blackbody and single temperature blackbody fit equally well with similar temperatures, we provide the parameters of the simpler black body model in Table 1 ($\chi^2/\nu = 0.8$ with $kT = 0.1$ keV and $N_H = 10^{22}$ cm $^{-2}$). Our data are insufficient to distinguish between these models. Because of the low number of counts, the errors on the spectral parameters were not better than a factor of 2. We note the large range of absorption and temperature values allowed by the fit ($0 < N_H < 3 \times 10^{22}$ cm $^{-2}$ and $0.04 < kT < 0.5$ keV).

Archival X-ray spectra for XRT-6 were extracted from both *XMM-Newton* and *Chandra* observations. The power-law model did not fit the spectra at all; therefore, we fit them with a blackbody model. The spectra, though taken at different times, proved to be similar, showing overlapping best-fit parameters for temperature and absorption. The observed 0.35-1.1 keV flux decreased from 1.2×10^{-13} erg cm $^{-2}$ s $^{-1}$ on 2000-Aug-2 to 2.9×10^{-14} erg cm $^{-2}$ s $^{-1}$ on 2000-Aug-4. Applying the same model to the *Chandra* spectrum from 2000-Aug-30 yields a flux of 6.0×10^{-14} erg cm $^{-2}$ s $^{-1}$. Column density - temperature confidence contours derived from the three spectra largely overlap, as shown in Figure 7, and a combined fit assuming constant temperature and column density yields $kT = 54 \pm 4$ eV and $N_H = 1.7(\pm 0.5) \times 10^{21}$ cm $^{-2}$, assuming elemental abundances from Anders & Grevesse (1989). Column densities in excess of $N_H \sim 1.9 \times 10^{21}$ cm $^{-2}$ are excluded if we assume an intrinsic source luminosity (0.2–2.4 keV, distance 795 kpc) for the 2000-Aug-02 observation below the Eddington limit (see also Pietsch et al. 2007). This absorption value is lower than that measured with the *Chandra* data alone (Grimm et al. 2007), possibly due to the better sensitivity of *XMM-Newton* at low energies or variable intrinsic absorption in the source.

We note that large extrapolation uncertainties go into estimating the bolometric lumi-

osity of a very soft source, making the estimate quite model-dependent (Heise et al. 1994). With more detailed spectra and more sophisticated modeling, the luminosity estimate for XRT-6 may decrease; however, such a decrease would require a decrease in the absorption correction. Therefore our measured upper-limit for the absorption column is secure against such changes in the spectral model. Furthermore, our absorption limit assumes the 0.2–2.4 keV X-ray luminosity as a conservative lower limit on the bolometric luminosity. We have restricted the luminosity estimate to the energy band that we actually observe, minimizing the model dependence of the estimate. Since the observed band is only a small fraction of the spectral energy distribution, our restriction on the column density is conservative. Better knowledge of the intrinsic source spectrum and bolometric luminosity would further decrease the upper limit for the column density.

We estimated the absorbed and unabsorbed 0.35–8 keV luminosities of the transient candidates with XSPEC, assuming the best-fit spectral model parameters. The unabsorbed values are shown in the light curves in Figure 3. Both values are provided for the observation with the greatest flux in Table 1. The photon fluxes given in the table were calculated before the spectra were fit and come from the exposure maps created by the ChASem33 team. They are meant to provide a consistent way of measuring the ratio of the highest to lowest observed flux and an important comparison between the best-fitting spectral parameters and the hardness ratios.

3.2. Timing

Although our temporal sampling is somewhat erratic, it reveals some interesting characteristics of the transient candidates. In addition, the long-integration observations provide some sensitivity to short outbursts while the sources were active.

Our sampling covers the decay of M33 XRT-1 fairly well, as can be seen in the light curves of Figure 3. This source decayed by nearly a factor of 2 in just 4 days, suggesting an e -folding decay time of ~ 1 week. As the source was not detected at the 1.5σ level in the next observation, 58 days after the brightest detection, we can conservatively place a 58 day upper limit on the decay time of the source, which is typical for a Be HMXB (see examples in Laycock et al. 2003). The decay time of XRT-3 could not be constrained in a meaningful way from our data, but the rise time of XRT-3 appears to be rapid, increasing in flux by a factor of 7 in under 3 days and a factor of at least 11 in less than 6 days. Such a rise time is similar to that of Galactic LMXB transients and black hole binaries (e.g., Chen et al. 1997).

The long-term lightcurve for XRT-4 does not provide clear evidence that it is a true

X-ray transient. It appears to be a faint, persistent source most of the time. In 2005, both of our non-detections have 1σ upper-limits near the bottom of the error bars of the detections, suggesting that the source was at a similar low flux during the shorter observations when it was not detected. There are no detections of the source in the *XMM-Newton* archival data, but the most sensitive observation at this location (observation 12a in Misanovic et al. 2006), taken 2000-Aug-02 provides an 0.2-4.5 keV absorbed luminosity upper-limit of 6×10^{35} erg s^{-1} , which is similar to the lower detected luminosities in the *Chandra* data. On the other hand, the source underwent an outburst in late June of 2006. It then decayed by a factor of 3 from 2006-Jun-26 to 2006-Jul-01. Furthermore, this source shows short-term variability, has a hard spectrum, and is associated with a blue optical counterpart candidate, making it a possible HMXB transient X-ray source.

The candidates XRT-5 and XRT-7 do not have enough temporal coverage to sample rise or decay times. For these candidates, the fact that they were never detected by *XMM-Newton* offers some supporting evidence that these sources are transients, but again, the sensitivity of the *XMM-Newton* observations provides 0.2-4.5 keV absorbed luminosity upper limits of 5×10^{35} erg s^{-1} , which is only slightly below the brightest detected luminosity in the *Chandra* data.

The *XMM-Newton* data for XRT-6 yield a short decay time, as the flux dropped by a factor of 4 in the 2 days between observations. These measurements suggest an e -folding decay time of ~ 1.3 days. However, the lightcurve of this transient candidate is clearly more complex than a simple exponential decay, as demonstrated by its flux in the *Chandra* observation 26 days after the *XMM-Newton* observations and by its short-term variability.

The K-S tests for short-term variability (i.e. flares or bursts within a single observation) of XRT-1, XRT-3, XRT-5, and XRT-7 gave probabilities of 0.1 or higher that the source was constant during the observation with the most counts. On the other hand, the sources XRT-2, XRT-4 and XRT-6 each showed evidence for short term variability while they were active. Our K-S test provides probabilities of only 2.2×10^{-2} , 4.4×10^{-3} and 6×10^{-9} that XRT-2, XRT-4 and XRT-6 had constant flux during ObsIDs 6376, 6387, and 786, respectively. The photon arrival times from those ObsIDs are shown in Figure 8. While the distribution for XRT-2 hints at a higher flux early in the observation and XRT-4 exhibits a higher flux later in the observation, the most dramatic variability observed is that of XRT-6, which shows two distinct bursts during the observation. One burst lasted for ~ 4 hours, beginning 2 hours into the observation. After a 2 hour break, there was another burst that continued to the end of the observation. Furthermore, in the *XMM-Newton* data from the brightest detection (2000-Aug-02), the source exhibits strong variability with outbursts on timescales of 1000-2000 s. Similar variability was observed during the last third of the observation on

2000-Aug-04.

3.3. Optical and Infrared Counterparts

We searched several available data archives and published catalogs for counterparts for the transient X-ray sources at optical and infrared wavelengths. These included the Local Group Survey¹ (Massey et al. 2006), the CFHT M33 survey² (Hartman et al. 2006), the DIRECT project³ (Macri et al. 2001), and the Wise Observatory M33 survey⁴ (Shporer & Mazeh 2006) catalogs, as well as imaging from the *Spitzer* data archive (see section § 2.3).

Several of the new potential X-ray transients have good optical counterpart candidates (Figure 9). This fact suggests that the sample contains several HMXBs. Galactic transient LMXBs typically have $-2 < M_V < 5$ ($22.5 < m_V < 29.5$ in M33) *in outburst* and are fainter in quiescence (van Paradijs & McClintock 1994), making LMXBs in M33 difficult to detect in ground-based imaging. Nevertheless, both XRT-1 and XRT-4 are within $2''$ of a bright blue star in the Massey et al. (2006) M33 catalog (IDs J013241.31+303220.0 and J013341.33+303212.6), and three of the other transient candidates have blue or variable stars within their 3σ error circles.

There are also transients that have good mid-infrared counterpart candidates. At these wavelengths, light from the donor star dominates the emission (e.g., Shahbaz et al. 1996). We therefore expect these systems to look like single stars, as is the case with all but one of the counterpart candidates.

3.3.1. Optical Counterparts

The magnitude ($V = 20.29$) and color ($B - V = 0.03$) of the XRT-1 counterpart suggest that the star is a moderately extinguished ($E_{B-V} \sim 0.28$) late O or early B star in M33. This counterpart candidate is not in a crowded region of M33, making the identification surprisingly clear. Furthermore, this star is known to be variable (CFHT 250258, D33 J013341.3+303212.7; Hartman et al. 2006; Macri et al. 2001) Although the X-ray posi-

¹<http://www.lowell.edu/~massey/lgsurvey/>

²<http://www.astro.livjm.ac.uk/~dfb/M33/>

³<http://cfa-www.harvard.edu/~kstanek/DIRECT/>

⁴<http://wise-obs.tau.ac.il/~shporer/m33/>

tion is off the star by approximately $2''$, the X-ray position is not tightly constrained because the source is on the detector edge. The X-ray position is off to the southeast, and the detection is on the northwest edge of the ACIS-I detector, as shown in Figure 4. Therefore any flux that could have fallen farther to the northwest would have been off the detector edge. The fact that the point spread function of the source spills over the detector edge to the northwest increases the likelihood that the *Chandra* position is skewed to the southeast.

The only cataloged star within the XRT-2 3σ error circle ($1.6''$) is J013332.34+303954.9 in the Massey et al. (2006) catalog. This is a faint blue star with $V = 22.8$ and $B - V = 0.1$. With this brightness and color, the star could be a moderately extinguished early B star in M33. If this star is the counterpart, XRT-2 would also be a HMXB, a reasonable possibility since this transient is recurrent and has a fairly hard spectrum ($\Gamma \sim 1.6$).

For XRT-3, the nearest optical counterpart is an uncataloged blue star within the error circle. This star is indicated with the arrow in Figure 9. We performed aperture photometry on this object and a neighboring star in the Massey et al. (2006) catalog using the images from the Local Group Survey. After correcting our magnitudes so that our photometry for the cataloged star matched those of Massey et al. (2006), the star has $V = 23.3$ and $B - V = -0.1$, making it a moderately extinguished B star in M33. Therefore XRT-3 may be another HMXB transient; however, the soft X-ray spectrum is not consistent with an HMXB transient. On the other hand, another potential optical counterpart is another known variable star (CFHT 320133). Photometry from the Massey et al. (2006) catalog (ID J013339.13+302113.2, $V = 20.36$) shows that it is quite red ($B - V = 2.00$). The star is redder than low-mass dwarfs, making the foreground reddening toward M33 inadequate to explain its color. The star is therefore a good candidate for an extinguished red supergiant or red helium-burning star in M33. As is the case with XRT-1, this source is also near the detector edge. In this case it is near the southeast edge of the detector (see Figure 4), increasing the likelihood that some flux spilled off the southeast edge of the detector, skewing the position to the northwest. The X-ray position is misaligned with the position of the star in this direction, increasing the plausibility that this star is the true counterpart, but this candidate is less certain than that of XRT-1 due to the higher density of stars in the area and the blue candidate closer to the measured X-ray position. From the density of variable stars with $1'$ of XRT-3 in the Hartman et al. (2006) catalog ($0.0095 \text{ arcsec}^{-2}$), the probability of finding a random variable star within $2''$ of XRT-3 is 0.12.

The XRT-4 counterpart candidate is likely a bit higher in mass; with $V = 18.13$ and $B - V = -0.18$, it is likely a late O supergiant. In addition, this counterpart candidate shows periodic variability with $P = 20.16$ days (W21058; Shporer & Mazeh 2006). Although the positional agreement of XRT-4 with the optical counterpart candidate is also only $1.5''$, the

optical variability and the hardness of the X-ray spectrum make this star a good counterpart candidate.

There is a variable optical counterpart candidate for XRT-5 (CFHT 144719; Hartman et al. 2006) inside of the 3σ error circle, $1.1''$ south of the X-ray position. This star was not included in the Massey et al. (2006) catalog, but has $\langle g \rangle = 22.4$ and $\langle g - r \rangle = 0.5$. This brightness and color allows the possibility that this star is in the Galactic halo, but the bright mid-IR counterpart (see § 3.3.2) suggests the presence of a highly absorbed object. If so, then XRT-5 could be a heavily extinguished HMXB in M33.

There are no clear optical counterpart candidates for XRT-6 or XRT-7. XRT-6 appears to have some optical emission within its error circle, but no stars have been cataloged at this position, suggesting the counterpart is too crowded to be measured in ground-based data. The area surrounding XRT-7 shows no B -band emission at all in the Massey et al. (2006) images.

The optical counterparts provide some insight into the bright transient population of M33. Apparently, at least 2 (and possibly five) of the transients (XRT-1, XRT-4, and possibly XRT-2, XRT-3 and/or XRT-5) are HMXBs. This result demonstrates a difference between M33 and the other earlier and more massive spirals of the Local Group, M31 (Williams et al. 2006b) and the Galaxy (Chen et al. 1997). The bright transient population of M33 is not dominated by LMXBs, and in fact may contain a large fraction of HMXBs. Since HMXBs are more short-lived than LMXBs, this low LMXB transient fraction suggests a more dominant young population, reflecting the later morphology of M33.

3.3.2. Infrared Counterparts

In Figure 10 we present images of the X-ray transient candidates showing counterparts in the IRAC data. The positions of the X-ray transient candidates are marked on each image. Transient candidates 1, 3, and 6 do not show obvious mid-IR emission and were not detected by SExtractor. Sources XRT-2, XRT-4 and XRT-5 were detected only in the first two IRAC channels, while source XRT-7 is detected in all four channels.

Using the photometric measurements (Table 2) we computed the IRAC colors $[3.6] - [4.5]$ and $[5.8] - [8.0]$. Three infrared counterpart candidates (XRT-2, XRT-4, XRT-5) show colors that are consistent with either constant or declining flux (F_ν) with increasing wavelength, though without detections in all four bands we are unable to better determine whether these objects are stellar sources within M33 or background galaxies from their fluxes alone. On the other hand, comparing the colors of XRT-7 with those of sources detected in the IRAC

shallow survey (Stern et al. 2005) we find that the colors of this object ($[3.6] - [4.5] = 1.1 \pm 0.6$, $[5.8] - [8.0] = 1.0 \pm 0.5$) strongly suggest that it is an AGN. The lack of optical emission and high X-ray absorption from XRT-7 are also consistent with an obscured AGN. This infrared counterpart therefore rules out the possibility that another transient (XRT-7) is a LMXB, leaving only 3 of 7 transients with the potential of being LMXBs.

The sizes of the mid-IR counterparts can also help in the determination of the object type. Although the large pixels and PSF of *Spitzer* make blending an obvious problem, one of the infrared counterparts was much larger than the *Spitzer* PSF. The counterpart of XRT-2 was measured to have a full-width at half-maximum of 7.9 pixels ($9.5''$) at $3.6 \mu\text{m}$. The size reduces to $6.5''$ at $4.5 \mu\text{m}$, which is still more than double the IRAC PSF ($\sim 2.5''$). The region is clearly very crowded in the *Spitzer* data, but of all of our counterparts, this one appears most likely to be extended. Such an extended mid-IR source could be unresolved stars in M33, which would be consistent with the large difference in size in different bandpasses, or a background galaxy. However, the likelihood of a background galaxy is low considering the X-ray variability and moderate absorption measured. Therefore, we suggest that this counterpart is a blend of stars in M33, still consistent with the possibility that XRT-2 is an LMXB or an HMXB.

The combination of optical and IR properties of the counterparts can also be effective for constraining object type. XRT-4 is the only transient with a strong counterpart candidate in both the optical and mid-IR data, likely because XRT-4 has the brightest optical counterpart candidate, which is probably a supergiant star. Fainter blue stars (such as the counterparts for XRT-1 and XRT-3) would require deeper IR imaging to detect. The lack of a clear, bright optical or IR candidate for XRT-3 is consistent with the possibility that it is a LMXB. On the other hand, the counterparts for XRT-2 and XRT-5 are detected. XRT-2 could be in a small cluster that is extincted. This would explain the bright and extended appearance in the mid-IR, but the faint appearance in the optical. XRT-5 has the reddest variable optical counterpart, which may explain its appearance in the mid-IR images. If the source is located in M33, it must be heavily absorbed and have an IR excess to explain its bright mid-IR fluxes as seen in the *Spitzer* data. Such IR excesses are common in *Be* systems (Cote & Waters 1987), allowing the possibility that XRT-5 is an HMXB, despite its relatively soft X-ray spectrum.

4. Conclusions

We have discovered 6 new candidate transient X-ray sources in M33; one of which (XRT-2) is a recurring transient source. A seventh previously-known transient was also found by

our search technique. These sources vary by at least a factor of 8 in flux in the *Chandra* observations considered here, and their spectra suggest they belong to a few different classes. For example, XRT-1 and XRT-4 are hard sources similar to HMXB transients. In contrast, XRT-2, XRT-5, and XRT-7 have soft spectra that are well-fitted by a power-law model. XRT-3 has an even softer spectrum similar to those of LMXB transients in the high state, and XRT-6 is a known SSS.

Optical counterpart candidates for XRT-1, XRT-2, XRT-3, XRT-4, and XRT-5 were identified from the DIRECT (Macri et al. 2001), Massey et al. (2006), Shporer & Mazeh (2006), and CFHT (Hartman et al. 2006) catalogs. The density of other faint stars near the locations of XRT-2, XRT-3, and XRT-5 make their counterpart candidates less reliable than the bright counterpart candidates of XRT-1 and XRT-4. These two candidates are bright blue variable stars, strongly suggesting that XRT-1 and XRT-4 are HMXBs.

Infrared counterparts of XRT-2, XRT-4, XRT-5, and XRT-7 were detected in *Spitzer* images of M33. The mid-IR color of XRT-7 suggests it is an AGN, consistent with its highly absorbed X-ray spectrum and the lack of an optical counterpart candidate. The mid-IR counterpart for XRT-2 has a color typical of stars, but it is extended, possibly because of crowding. The mid-IR counterpart of XRT-4 is consistent with being the same bright star seen in the optical. The mid-IR counterpart of XRT-5 also has the color of a star, but it is bright compared to the optical counterpart candidate, suggesting the optical counterpart is heavily extinguished. If so, XRT-5 is another good HMXB transient candidate.

Our multi-wavelength measurements allow the possibility that at most three (XRT-2, XRT-3 and XRT-5) of these 6 sources could be LMXBs. While these three transients are particularly difficult to classify, only XRT-3 has no mid-IR counterpart and is much softer than expected for an HMXB. Therefore XRT-3 is the best LMXB candidate in our sample.

Although our sparse sampling does not allow us to constrain the transient rates or duty cycles, the source types and locations allow for some interesting comparisons with the Galaxy and M31. Apparently, the transient population of M33 is not dominated by LMXBs. This low LMXB fraction is different from the bright X-ray transients in M31, where most are found in the bulge (Williams et al. 2006b) and have optical counterparts consistent with LMXBs (Williams et al. 2006a). On the other hand, the M31 transients are similar to those of the Galaxy. For example, the distributions of transient peak luminosities and decay times in M31 are very similar to those of the Galaxy (Williams et al. 2006b; Chen et al. 1997). Our results now suggest that these populations are somewhat different from that of M33, whose brightest transients appear to be spread over the whole galaxy and to contain a significant fraction of HMXBs. M33 is known to be a later-type, more intensely star-forming galaxy than M31 or the Galaxy. These morphological differences are reflected in the metallicities,

stellar populations, and apparently the bright X-ray transient populations of the galaxies.

Finally, the potential of some of these sources for containing stellar-mass black holes makes their discovery of particular interest for studies of black hole formation and accretion. The final catalog of sources from the ChASeM33 data is currently under construction, and our search for transients will be extended to include all of those sources contained in the full survey data set when the final source catalog is available.

Support for this work was provided by the National Aeronautics and Space Administration through *Chandra* Award Numbers G06-7073A and GO6-7073B issued by the *Chandra* X-ray Observatory Center, which is operated by the Smithsonian Astrophysical Observatory for and on behalf of the National Aeronautics Space Administration under contract NAS8-03060. We also acknowledge the images from the Local Group Survey⁵, which were used to prepare the optical finding charts for the transient sources.

REFERENCES

- Anders, E. & Grevesse, N. 1989, *Geochim. Cosmochim. Acta*, 53, 197
- Bertin, E. & Arnouts, S. 1996, *A&AS*, 117, 393
- Block, D. L., Combes, F., Puerari, I., Freeman, K. C., Stockton, A., Canalizo, G., Jarrett, T. H., Groess, R., Worthey, G., Gehrz, R. D., Woodward, C. E., Polomski, E. F., Fazio, G. G., & –. 2007, *ArXiv e-prints*, 706
- Broos, P., Townsley, L., Getman, K., & Bauer, F. 2002, *ACIS Extract, An ACIS Point Source Extraction Package*, Pennsylvania State University
- Chen, W., Shrader, C. R., & Livio, M. 1997, *ApJ*, 491, 312
- Coe, M. J., Negueruela, I., Buckley, D. A. H., Haigh, N. J., & Laycock, S. G. T. 2001, *MNRAS*, 324, 623
- Cote, J. & Waters, L. B. F. M. 1987, *A&A*, 176, 93
- Di Stefano, R., Kong, A. K. H., Greiner, J., Primini, F. A., Garcia, M. R., Barmby, P., Massey, P., Hodge, P. W., Williams, B. F., Murray, S. S., Curry, S., & Russo, T. A. 2004, *ApJ*, 610, 247++

⁵<http://www.lowell.edu/~massey/lgsurvey/>

- Fazio, G. G., Hora, J. L., Allen, L. E., Ashby, M. L. N., Barmby, P., Deutsch, L. K., Huang, J.-S., Kleiner, S., Marengo, M., Megeath, S. T., Melnick, G. J., Pahre, M. A., Patten, B. M., Polizotti, J., Smith, H. A., Taylor, R. S., Wang, Z., Willner, S. P., Hoffmann, W. F., Pipher, J. L., Forrest, W. J., McMurty, C. W., McCreight, C. R., McKelvey, M. E., McMurray, R. E., Koch, D. G., Moseley, S. H., Arendt, R. G., Mentzell, J. E., Marx, C. T., Losch, P., Mayman, P., Eichhorn, W., Krebs, D., Jhabvala, M., Gezari, D. Y., Fixsen, D. J., Flores, J., Shakoorzadeh, K., Jungo, R., Hakun, C., Workman, L., Karpati, G., Kichak, R., Whitley, R., Mann, S., Tollestrup, E. V., Eisenhardt, P., Stern, D., Gorjian, V., Bhattacharya, B., Carey, S., Nelson, B. O., Glaccum, W. J., Lacy, M., Lowrance, P. J., Laine, S., Reach, W. T., Stauffer, J. A., Surace, J. A., Wilson, G., Wright, E. L., Hoffman, A., Domingo, G., & Cohen, M. 2004, *ApJS*, 154, 10
- Gaetz, T. J., Blair, W. P., Hughes, J. P., Winkler, P. F., Long, K. S., Pannuti, T. G., Williams, B., Edgar, R. J., Ghavamian, P., Plucinsky, P. P., Sasaki, M., Kirshner, R. P., Avillez, M., & Breitschwerdt, D. 2007, *ApJ*, 663, 234
- Gehrels, N. 1986, *ApJ*, 303, 336
- Grimm, H. ., McDowell, J., Zezas, A., Kim, D. ., & Fabbiano, G. 2007, *ArXiv e-prints*, 706
- Grimm, H.-J., McDowell, J., Zezas, A., Kim, D.-W., & Fabbiano, G. 2005, *ApJS*, 161, 271
- Haberl, F. & Pietsch, W. 2004, *A&A*, 414, 667
- Hartman, J. D., Bersier, D., Stanek, K. Z., Beaulieu, J.-P., Kaluzny, J., Marquette, J.-B., Stetson, P. B., & Schwarzenberg-Czerny, A. 2006, *MNRAS*, 371, 1405
- Hatzidimitriou, D., Pietsch, W., Misanovic, Z., Reig, P., & Haberl, F. 2006, *A&A*, 451, 835
- Heise, J., van Teeseling, A., & Kahabka, P. 1994, *A&A*, 288, L45
- Jain, R. K., Bailyn, C. D., Orosz, J. A., McClintock, J. E., & Remillard, R. A. 2001, *ApJ*, 554, L181
- Jester, S., Schneider, D. P., Richards, G. T., Green, R. F., Schmidt, M., Hall, P. B., Strauss, M. A., Vanden Berk, D. E., Stoughton, C., Gunn, J. E., Brinkmann, J., Kent, S. M., Smith, J. A., Tucker, D. L., & Yanny, B. 2005, *AJ*, 130, 873
- Kahabka, P. & Pietsch, W. 1996, *A&A*, 312, 919
- King, A. R., Osborne, J. P., & Schenker, K. 2002, *MNRAS*, 329, L43

- Laycock, S., Coe, M. J., Wilson, C. A., Harmon, B. A., & Finger, M. 2003, MNRAS, 338, 211
- Macri, L. M., Stanek, K. Z., Sasselov, D. D., Krockenberger, M., & Kaluzny, J. 2001, AJ, 121, 870
- Massey, P., Olsen, K. A. G., Hodge, P. W., Strong, S. B., Jacoby, G. H., Schlingman, W., & Smith, R. C. 2006, AJ, 131, 2478
- McClintock, J. E. & Remillard, R. A. Black hole binaries (Compact stellar X-ray sources), 157–213
- Misanovic, Z., Pietsch, W., Haberl, F., Ehle, M., Hatzidimitriou, D., & Trinchieri, G. 2006, A&A, 448, 1247
- Pietsch, W., Haberl, F., Sala, G., Stiele, H., Hornoch, K., Riffeser, A., Fliri, J., Bender, R., Bühler, S., Burwitz, V., Greiner, J., & Seitz, S. 2007, A&A, 465, 375
- Pietsch, W., Haberl, F., Sasaki, M., Gaetz, T. J., Plucinsky, P. P., Ghavamian, P., Long, K. S., & Pannuti, T. G. 2006, ApJ, 646, 420
- Pietsch, W., Misanovic, Z., Haberl, F., Hatzidimitriou, D., Ehle, M., & Trinchieri, G. 2004, A&A, 426, 11
- Plucinsky, P. P., Williams, B., Long, K. S., Gaetz, T. J., Sasaki, M., Pietsch, W., Tüllmann, R., Smith, R. K., Blair, W. P., Helfand, D., Hughes, J. P., Winkler, P. F., de Avillez, M., Bianchi, L., Breitschwerdt, D., Edgar, R. J., Ghavamian, P., Grindlay, J., Haberl, F., Kirshner, R., Kuntz, K., Mazeh, T., Pannuti, T. G., Shporer, A., & Thilker, D. A. 2008, ApJS, 174, 366
- Reach, W. T., Megeath, S. T., Cohen, M., Hora, J., Carey, S., Surace, J., Willner, S. P., Barmby, P., Wilson, G., Glaccum, W., Lowrance, P., Marengo, M., & Fazio, G. G. 2005, PASP, 117, 978
- Shahbaz, T., Bandyopadhyay, R., Charles, P. A., & Naylor, T. 1996, MNRAS, 282, 977
- Shporer, A. & Mazeh, T. 2006, MNRAS, 370, 1429
- Stern, D., Eisenhardt, P., Gorjian, V., Kochanek, C. S., Caldwell, N., Eisenstein, D., Brodwin, M., Brown, M. J. I., Cool, R., Dey, A., Green, P., Jannuzi, B. T., Murray, S. S., Pahre, M. A., & Willner, S. P. 2005, ApJ, 631, 163
- Tanaka, Y. & Shibazaki, N. 1996, ARA&A, 34, 607

- Tomsick, J. A., Corbel, S., Goldwurm, A., & Kaaret, P. 2005, *ApJ*, 630, 413
- van den Bergh, S. 1991, *PASP*, 103, 609
- van Paradijs, J. & McClintock, J. E. 1994, *A&A*, 290, 133
- Williams, B. F., Garcia, M. R., Kong, A. K. H., Primini, F. A., King, A. R., Di Stefano, R., & Murray, S. S. 2004, *ApJ*, 609, 735++
- Williams, B. F., Garcia, M. R., McClintock, J. E., Primini, F. A., & Murray, S. S. 2006a, *ApJ*, 637, 479
- Williams, B. F., Naik, S., Garcia, M. R., & Callanan, P. J. 2006b, *ApJ*, 643, 356
- Zaritsky, D., Elston, R., & Hill, J. M. 1989, *AJ*, 97, 97

Table 1. The Properties of the candidate transient X-ray sources

	XRT-1	XRT-2	XRT-3	XRT-4
ChASem33 number	10	130	161	171
R.A. (J2000)	01 32 41.35	01:33:32.23	01 33 38.90	01 33 41.26
Dec. (J2000)	+30 32 18.2	+30:39:55.8	+30 21 14.0	+30 32 13.5
Position Error (″)	0.52 ^k	0.22	0.68 ^l	0.28
Total Net Counts ^a	119	229	34	229
Photon Index (Γ)	0.7±0.4	1.6±0.4	...	0.6 ^{+0.5} _{-0.3}
kT (keV)	0.1;	...
N_H (10^{22} cm ⁻²)	0.2;	0.1;	1;	0.2 ^{+0.6} _{-0.2}
χ^2/ν	1.9	1.4	0.8	0.8
DOF	3	10	4	11
Soft ^b	2.8±2.1	7.1±1.3	10.6±5.5	3.3±1.1
Med ^c	5.8±1.1	6.2±0.7	8.5±2.4	5.5±0.7
Hard ^d	13.8±2.5	6.5±1.0	-1.1±3.1	14.4±1.5
Date of Max	2005-Sep-26	2005-Nov-23	2005-Oct-01	2006-Jun-26
Max flux ^e	6.6±1.0	2.1±0.3	5.3±1.2	3.5±0.4
Max lum ^f	23	6	4	18
Max unabsorbed lum ^g	25	7	830	19
Min Date	2006-Jun-15	2000-Jul-12	2005-Sep-26	2005-Nov-21
Min flux ^h	<6.6	<2.6	<4.8	<4.1
Max/Min ⁱ	>10	>8	>11	>9
Decay Time (days)	5 < t_d < 58
Rise Time (days)	$t_r < 6$...
m_V	20.29	22.8	23.3	18.1
$B - V$	0.03	0.11	-0.1	-0.2
<i>XMM-Newton</i> ? ^j	NO	[MPH2006] 145	[MPH2006] 162?	[MPH2006] 168?

Table 1. The Properties of the candidate transient X-ray sources

	XRT-5	XRT-6	XRT-7
ChASeM33 Number	241	...	393
R.A. (J2000)	01 34 01.64	01 34 09.92	01 35 09.11
Dec. (J2000)	+30 48 29.8	+30 32 19.9	+30 43 41.5
Position Error (")	0.17	0.40	0.43
Counts ^a	226	606 ^m	53
Photon Index (Γ)	$1.9^{+0.6}_{-0.4}$...	$2.0^{+2.0}_{-1.3}$
kT (keV)	...	0.054 ± 0.004	...
N_H (10^{22} cm^{-2})	$0.3^{+0.3}_{-0.2}$	0.17 ± 0.05	$0.9^{+1.5}_{-0.9}$
χ^2/ν	1.2	2.0	0.2
DOF	10	22	3
Soft ^b	7.3 ± 1.5	35.9 ± 2.7	1.0 ± 1.8
Med ^c	8.6 ± 0.9	0.0 ± 0.2	5.0 ± 1.2
Hard ^d	7.5 ± 1.3	0.4 ± 0.6	5.8 ± 2.1
Date of Max	2006-Mar-03	2000-Aug-02	2006-Jun-09
Max flux ^e	3.1 ± 0.4	158 ± 13^n	2.1 ± 0.3
Max lum ^f	8	88	3
Max unabsorbed lum ^g	12	620	7
Date of Min	2001-Jul-06	2006-Jun-26	2001-Jul-06
Min flux ^h	<2.6	<14.5	<1.9
Max/Min ⁱ	>12	>109	>11
Decay Time (days)	...	1.3	...
Rise Time (days)
m_V	22.1°
$B - V$	0.7°
XMM-Newton? ^j	NO	[MPH2006] 207 (SSS)	NO

^aNet counts summed over all observations of the source.

^bAverage 0.35–1.1 keV photon flux from all observations in units of 10^{-7} photons $\text{cm}^{-2} \text{s}^{-1}$.

^cAverage 1.1–2.6 keV photon flux from all observations in units of 10^{-7} photons $\text{cm}^{-2} \text{s}^{-1}$.

^dAverage 2.6–8.0 keV photon flux from all observations in units of 10^{-7} photons $\text{cm}^{-2} \text{s}^{-1}$.

^eMaximum observed 0.35–8 keV photon flux in units of 10^{-6} photons $\text{cm}^{-2} \text{s}^{-1}$

^fMaximum observed 0.35–8 keV luminosity, assuming the best-fitting spectral model, in units of 10^{35} erg s^{-1} .

^gMaximum observed absorption-corrected 0.35–8 keV luminosity, assuming the best-fitting spectral model, in units of 10^{35} erg s^{-1} .

^hMinimum observed 0.35–8 keV photon flux in units of $\times 10^{-7}$ photons $\text{cm}^{-2} \text{s}^{-1}$.

ⁱLower-limit of the ratio of the maximum 0.35 – 8 keV flux of the source to the minimum 0.35–8 keV flux of the source.

^jWas the source included in the *XMM-Newton* catalogs of Pietsch et al. (2004) and/or Misanovic et al. (2006)?

^kThis random error does not include the effects of the chip edge, which may have skewed the source position as much as $2''$ to the southeast.

^lThis random error does not include the effects of the chip edge, which may have skewed the source position as much as $2''$ to the northwest.

^m254 counts from Aug. 2 *XMM-Newton*; 189 counts from Aug. 4 *XMM-Newton*; 163 counts from Aug. 30 *Chandra*.

ⁿPhoton flux taken from simultaneous spectral fitting (see § 3.1).

^oMagnitudes converted from g and r to B and V using the transformations of Jester et al. (2005).

Table 2. Magnitudes^a and Colors of Mid-Infrared Counterparts to X-ray Transient Candidates in M33

ID	m _{3.6}	m _{4.5}	m _{5.8}	m _{8.0}	[3.6]–[4.5]	[5.8]–[8.0]
XRT-1
XRT-2	15.0 ± 0.2	14.8 ± 0.2	0.2 ± 0.3	...
XRT-3
XRT-4	15.5 ± 0.3	15.6 ± 0.3	–0.1 ± 0.4	...
XRT-5	16.2 ± 0.4	16.0 ± 0.4	15.0 ± 0.5	...	0.2 ± 0.6	...
XRT-6
XRT-7	16.9 ± 0.5	15.8 ± 0.4	15.0 ± 0.3	14.0 ± 0.3	1.1 ± 0.6	1.0 ± 0.5

^aComputed according to the Vega-magnitude system as described for IRAC by Reach et al. (2005).

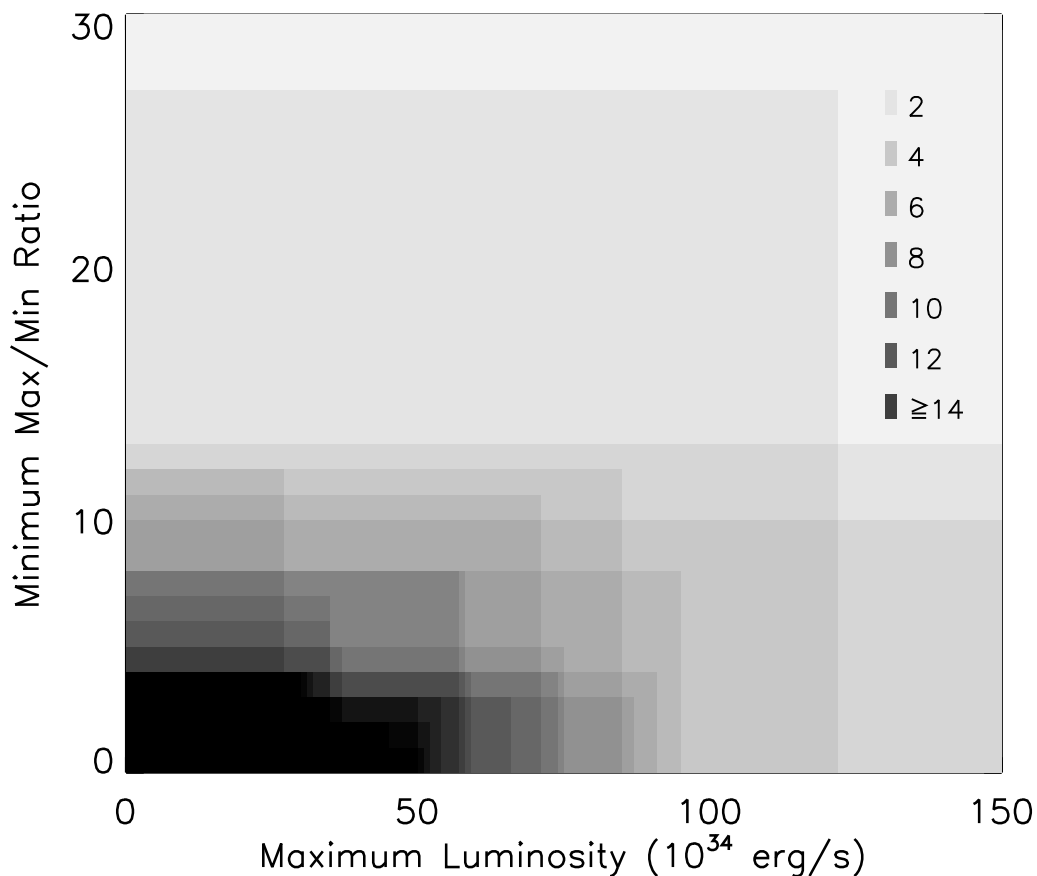


Fig. 1.— Grayscale plot of the effects of changing the maximum luminosity and flux ratio (h/l) selection criteria for finding transient candidates (see discussion in § 2.1). Dark areas denote larger numbers of sources passing the criteria. The key in the upper-right of the plot gives the number of sources represented by some of the gray tones. The sharp increase in number of sources passing the search criteria when the maximum observed luminosity criterion is set below about 4×10^{35} erg s $^{-1}$ and the h/l criterion is set below about 8 helped us determine the criteria to use for initially flagging sources for follow-up analysis.

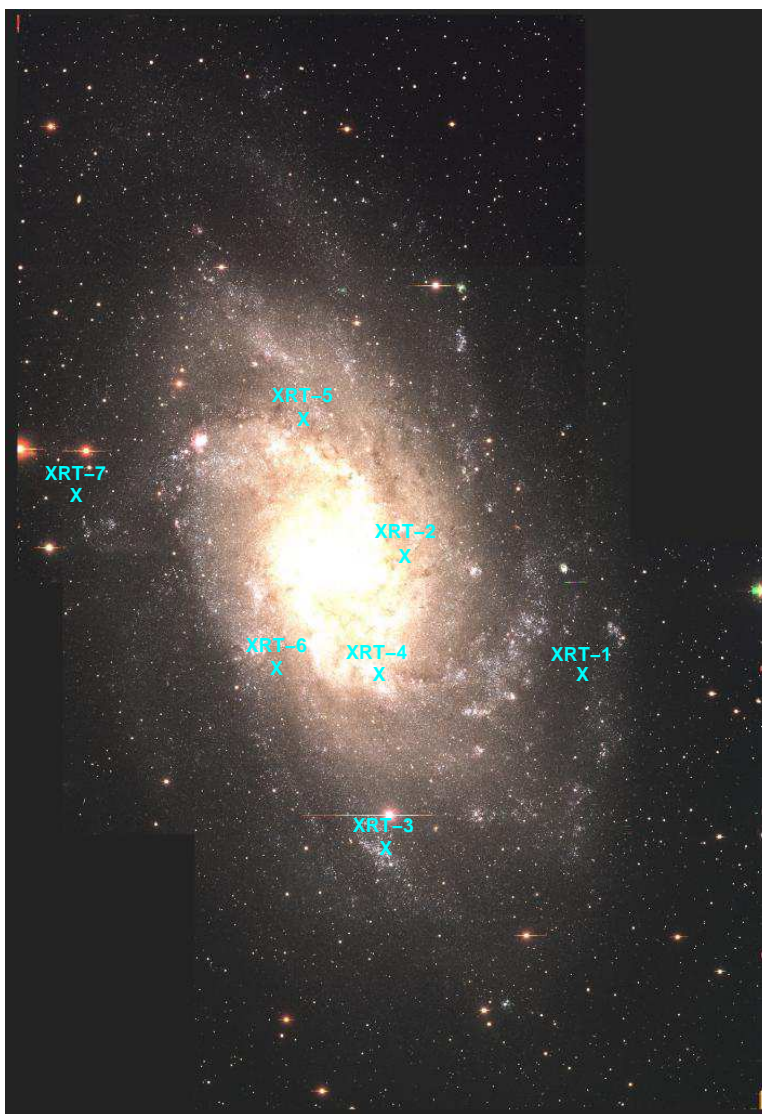


Fig. 2.— The locations of our 7 X-ray transient candidates are shown on the Local Group Galaxy Survey image of M33 (Massey et al. 2006).

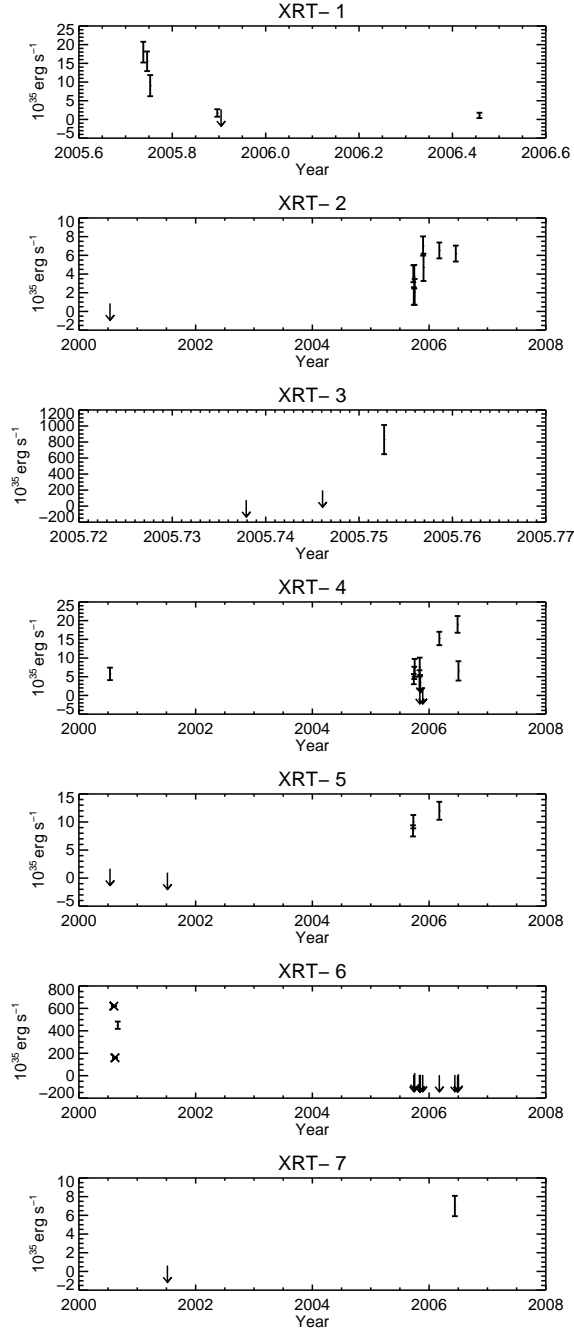


Fig. 3.— X-ray light curves for the 7 transient candidates. Luminosities measured from archival *XMM-Newton* data are marked with the X symbol. Error bars show standard deviation calculated from photon statistics only and are appropriate for comparing the relative measured fluxes for each source. Absolute luminosities assume the chosen spectral model detailed in Table 1 is correct and therefore have much larger uncertainties. Each source shows an outburst that is more than 8 times brighter than its faintest upper-limit.

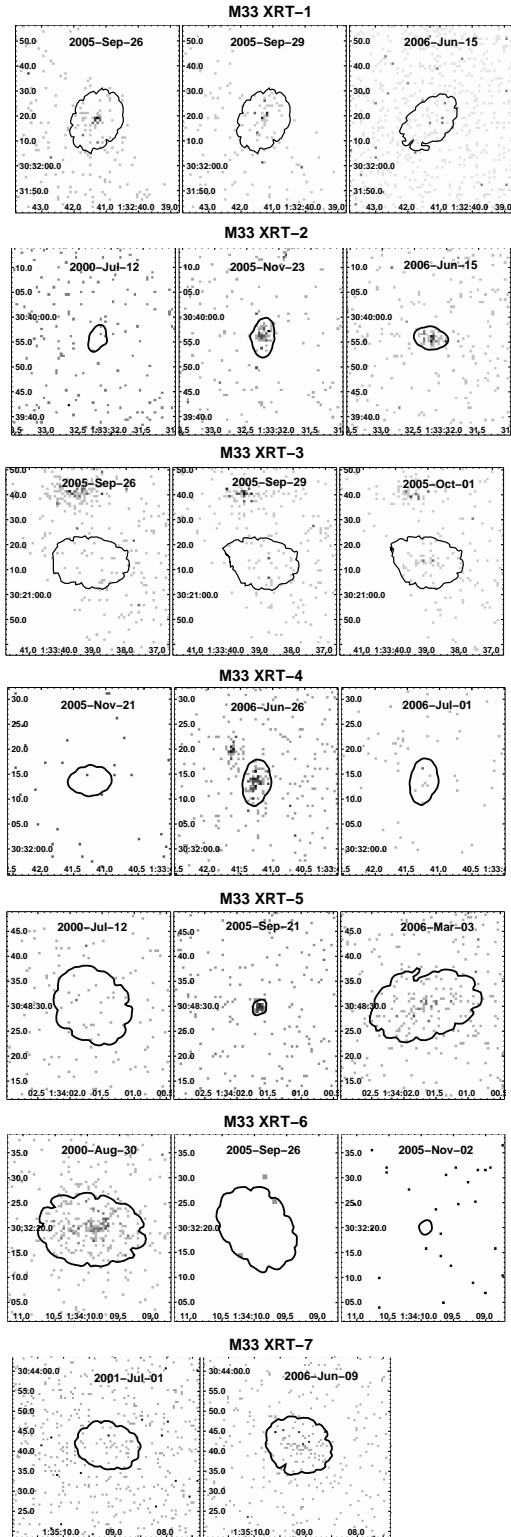


Fig. 4.— X-ray images of the 7 transient candidates at different times. The dates were chosen to sample on and off times for each candidate. The background levels are different for each observation due to the different exposure times.

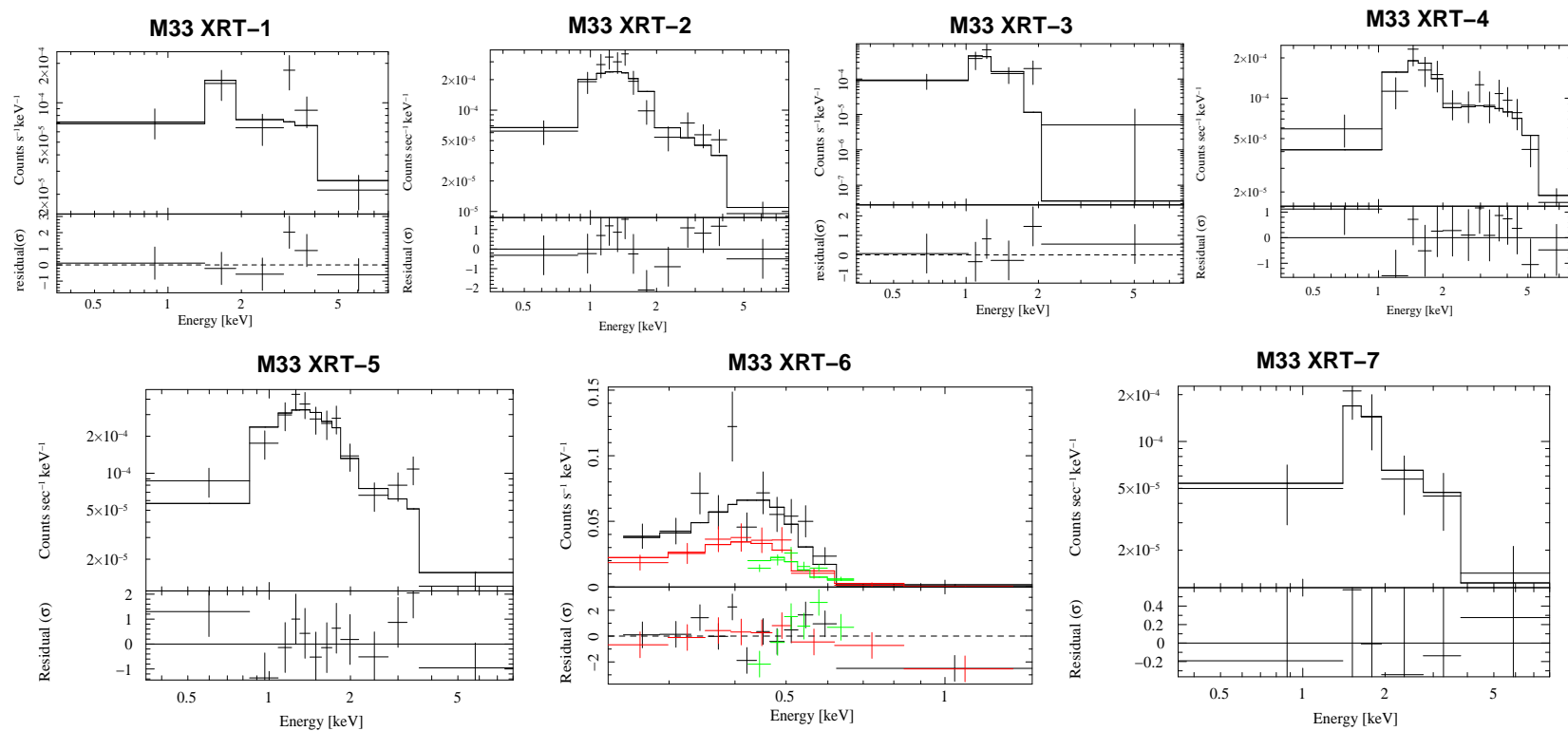


Fig. 5.— Spectral fits to the *Chandra* data for each transient candidate. XRT-1 and XRT-4 are significantly harder than the other candidates. Absorbed power-law model fits are shown except for XRT-3 and XRT-6, where absorbed blackbody model fits are shown. For XRT-6 (the SSS), the combined *Chandra* (green) and *XMM-Newton*-pn from August 2 (black) and August 4 (red) spectral fit is shown.

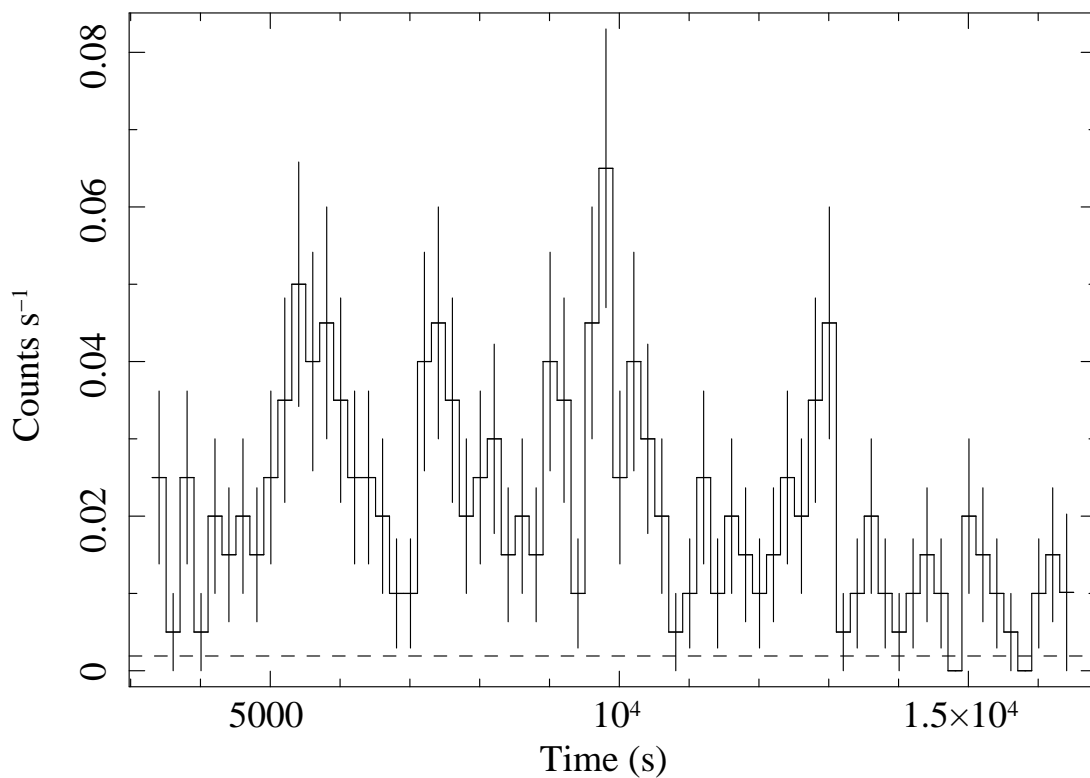


Fig. 6.— The *XMM-Newton* EPIC-pn light curve of XRT-6 during the 2000, Aug. 2 observation, showing several Short outbursts with time scales of 1000-2000 s. Single-pixel events were extracted in the 0.2-0.6 keV band. The average background level is indicated by the horizontal dashed line. Zero time refers to UT 06:56:39.

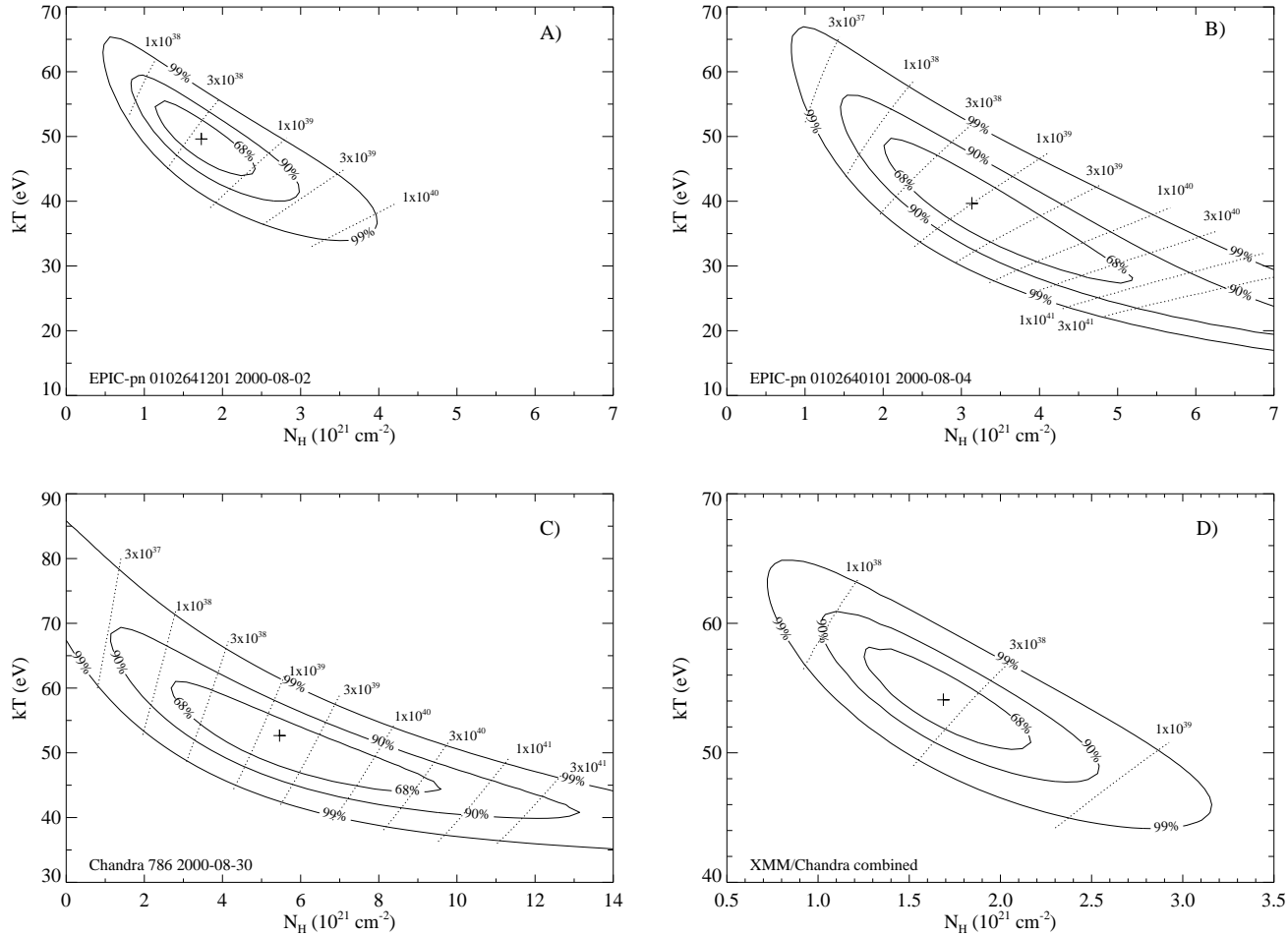


Fig. 7.— Column density - temperature confidence contours inferred from fits to the three spectra of XRT-6 using an absorbed blackbody model. The formal best fit parameter values are indicated by a cross. *A-B*: The fitting results for the individual *XMM-Newton* observations. Lines of constant 0.2-2.4 keV luminosity (in erg s^{-1}) are drawn on each plot, indicating the absorption-corrected luminosity of the source with those spectral parameters. *C*: The fitting results for *Chandra* observation. Lines of constant absorption-corrected 0.3-2.4 keV luminosity (in erg s^{-1}) are drawn on each plot. *D*: The results of a simultaneous fit to all of the spectra. Lines of constant absorption-corrected 0.2-2.4 keV luminosity (in erg s^{-1}) are drawn on each plot.

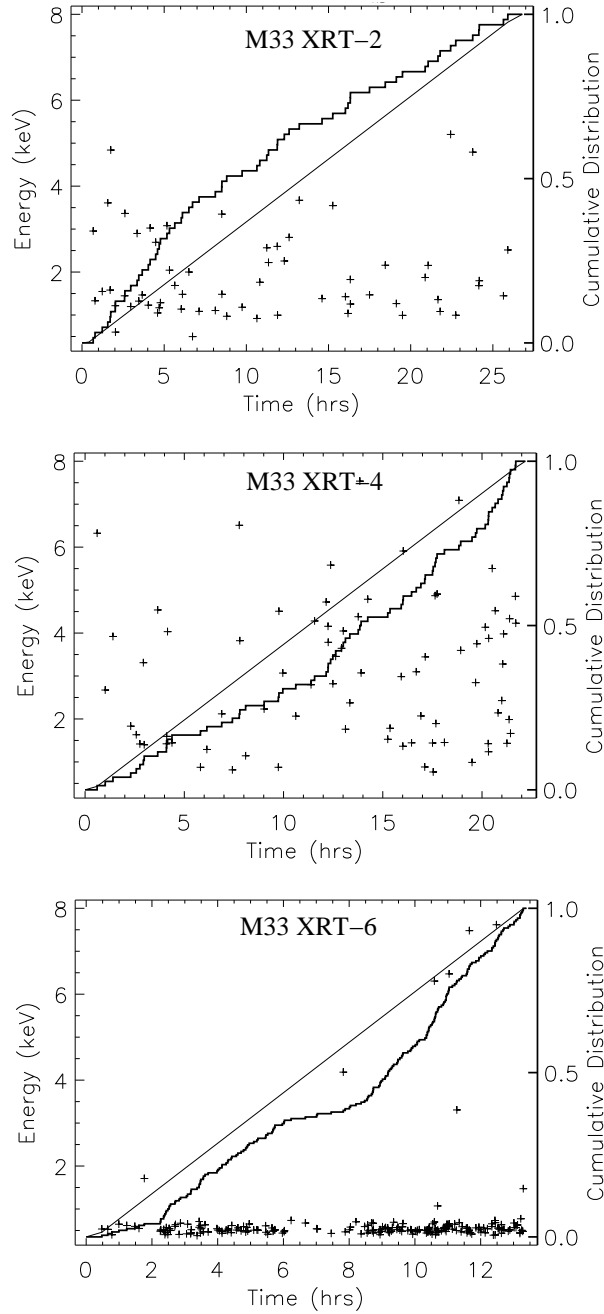


Fig. 8.— Unbinned photon arrival times for XRT-2, XRT-4 and XRT-6 during Observations 6376 (top), 6387 (middle) and 786 (bottom), respectively. Black points mark the time and energy of each detected photon. The histogram shows the cumulative fraction of detected photons, and the line marks the cumulative fraction expected for a source with constant flux.

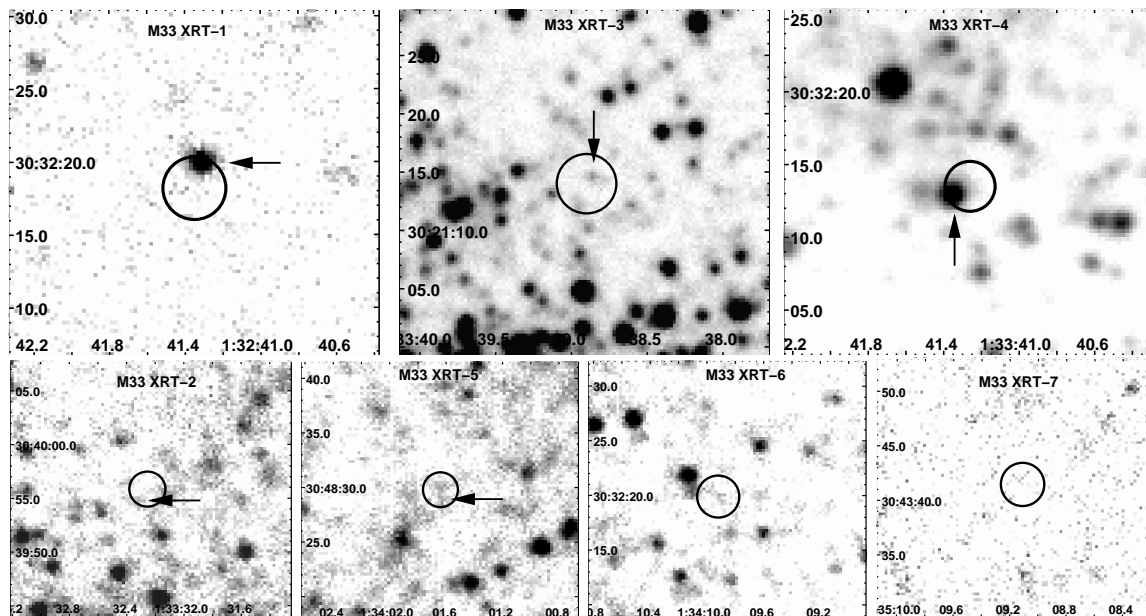


Fig. 9.— *B*-band images of the locations of the 7 transient candidates taken from the Local Group Survey (Massey et al. 2006). Circles are 3σ in radius (after adding $0.5''$ in quadrature to the X-ray position errors to account for X-ray - optical alignment). The best counterpart candidates from the Massey et al. (2006) data are indicated with arrows. Bright blue stars overlap the XRT-1 and XRT-4 circles. A bright red variable star (faint in the *B*-band image) is just outside the east side of the XRT-3 circle. Faint stars are cataloged just inside the error circles of XRT-2 and XRT-5. No clear counterpart candidates were found for XRT-6 or XRT-7.

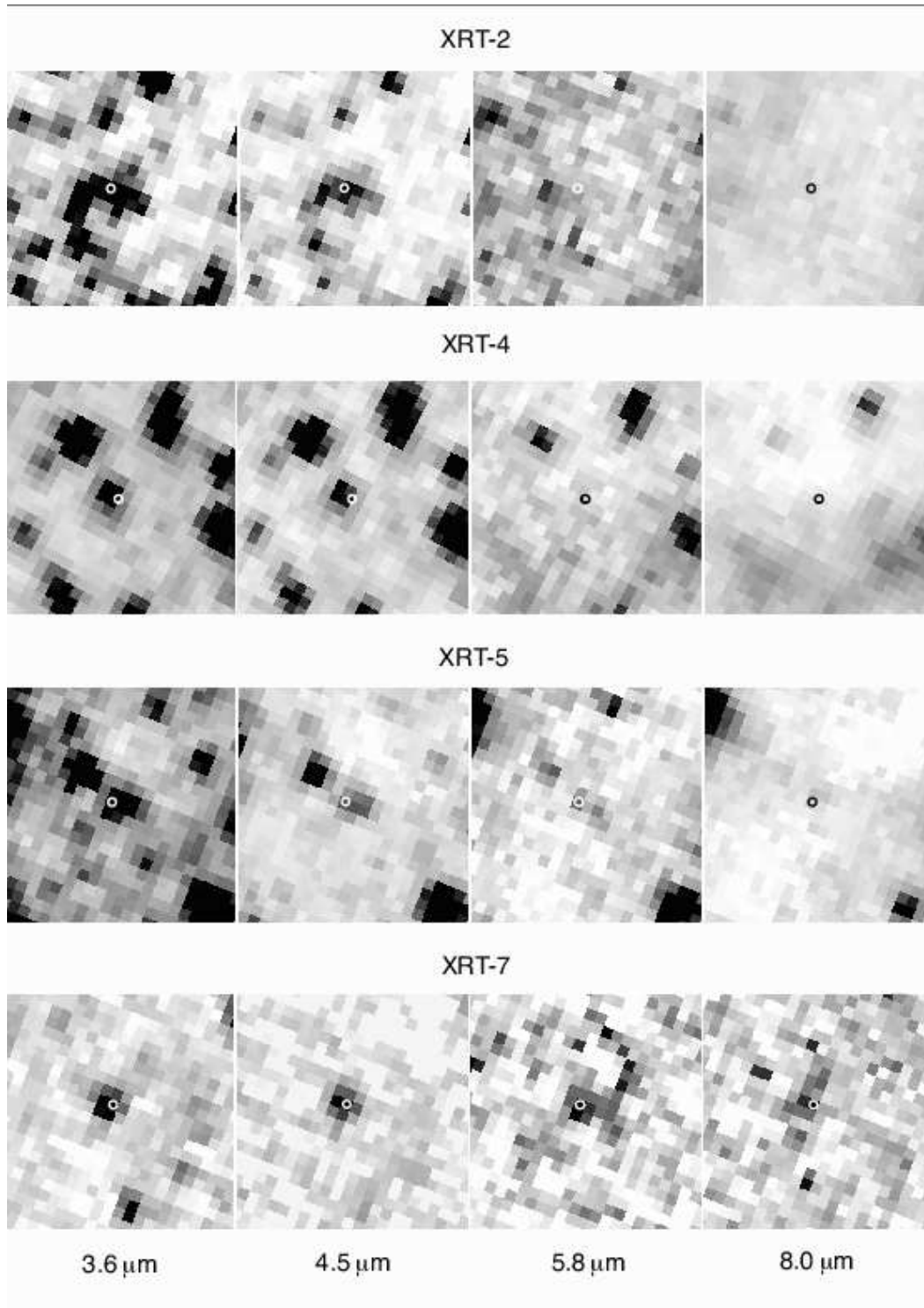


Fig. 10.— Mid-Infrared counterparts to the X-ray transient candidates in M33. The X-ray position of each source is marked on closeup images of all four IRAC channels. Each field is $25''$ square in size, with north at the top and east to the left. XRT-2 appears to be coincident with an extended source. XRT-2, XRT-4 and XRT-5 are co-incident with sources with blue IR colors similar to those of stars. XRT-7 has IR colors that are consistent with broad-line AGNs.